Reversible Immobilization of Proteins in Sensors and Solid-state Nanopores

Adithya Ananth[*1], *María Genua*[*2], *Nesrine Aissaoui*[*2], *Leire Díaz*[2], *Nico B. Eisele*[2], *Steffen Frey*[3,5], *Cees Dekker*[$1], *Ralf P. Richter*[$2,4] *and Dirk Görlich*[3]

[1] Department of Bionanoscience, Kavli Institute of Nanoscience, Delft University of Technology, Van der Maasweg 9, 2629 HZ Delft, The Netherlands

[2] CIC biomaGUNE, Biosurfaces Lab, Paseo Miramon 182, 20014 San Sebastian, Spain

[3] Max Planck Institute for Biophysical Chemistry, Am Fassberg 11, 37077 Göttingen, Germany

[4]University of Leeds, Faculty of Biological Sciences, School of Biomedical Sciences, Faculty of Mathematics and Physical Sciences, School of Physics and Astronomy, and Astbury Centre for Structural Molecular Biology, Leeds, LS2 9JT, United Kingdom

[5]Current address: NanoTag Biotechnologies GmbH, Rudolf-Wissell-Str. 28a, 37079 Göttingen, Germany

* These shared first authors contributed equally

[$] Corresponding authors. E-mails: r.richter@leeds.ac.uk, c.dekker@tudelft.nl

Abstract

The controlled functionalization of surfaces with proteins is crucial for many analytical methods in life science research and biomedical applications. Here we establish a coating for silica-based surfaces that enables stable and selective immobilization of proteins with controlled orientation and tunable surface density. The coating is reusable, retains functionality upon long-term storage in air, and is applicable to surfaces of complex geometry. We validate the protein anchoring method on planar SiO_2 and SiN surfaces, and then develop a method to measure the anchoring process in real time using SiN solid-state nanopores. For surface attachment, we exploit polyhistidine (His) tags that are site-specifically introduced into recombinant proteins, and use the yeast nucleoporin Nsp1 FG domain as model protein. Contrary to the commonly used covalent thiol chemistry, the anchoring of proteins *via* His tag is reversible, permitting to take proteins off and replace them by other ones. We monitor such switching in real time in experiments on individual nanopores using ion conductivity. Finally, we demonstrate that silica and gold surfaces can be orthogonally functionalized to accommodate His-tagged proteins on silica but prevent protein binding to gold, which extends the applicability of our surface functionalization method to even more complex sensor devices.

Keywords. Nanopore; Sensors; Surface functionalization; Histidine tag

1. Introduction

Functionalization of material surfaces with biomolecules with nanoscale control is required for a wide variety of applications. In biosensing devices, for example, nanopores are very promising tools for DNA sensing,[1] ion detection,[2] macromolecule/protein sensing,[3] DNA sequencing,[4] molecular separation,[5] and biomimetics.[6] Chemical modification of solid-state nanopores is a key task to control the functional groups at surfaces, and to give a specific function to the pores, designed for example for antifouling,[7] or more specifically for target applications.[8] Specific functionalization of the nanopores and other materials with complex surface geometry is challenging, however, partly because of the lack of analytical characterization techniques that can provide detailed information of the physico-chemical properties of the modified nanopores, required to control the degree, quality and spatial arrangement of the functionality.[7b, 9]

Planar surfaces, on the other hand, enable application of a broad range of surface-sensitive characterization techniques which provide a detailed description of the structure and physico-chemical properties of surface-confined biomolecular films and time-resolved information of film formation, reorganization processes, and of biomolecular interactions. This makes them ideal, as we demonstrate here, to tailor and quality control surface functionalization and protein immobilization approaches prior to their translation onto more complex surface geometries.

Nanopores in silicon-derived membranes can be tuned with subnanometer precision in size and shape.[10] The silicon-derived membranes present better mechanical, chemical and thermal characteristics compared with lipid-bilayer-based systems, and can be integrated with electronic or optical readout techniques.[11] SiN is the most popular material because of its low stress and excellent aspect ratio membranes for fabricating single nanopores with well-defined

shape and size, as well as high-density nanopore arrays.[5b, 10, 12] SiN pores can be covered with gold in order to use thiol chemistry to attach molecules.[8b, 13] However, silanes are most extensively used for the direct coating of nanopores in silicon-based solid-state membranes. Silanes have been used, for example, to modify the charge of the SiN pore surface for charge-based molecular differentiation.[5b] They can also be used as a platform to further covalently link other organic molecules, such as glutaraldehyde.[8a] Alternatively, the pore walls can be coated with biomolecules such as lipids, nucleic acids, or proteins. Yusko et al [14] showed the advantages of coating a nanopore with a lipid bilayer in terms of tuning protein translocation speeds, preventing non-specific adsorption, and attaching streptavidin-functionalized molecules by incorporation of biotin into the lipid bilayers. For nucleic acids or proteins, a molecular recognition element, like a single-stranded DNA for the detection of the complementary sequence, or an aptamer for complementary shape recognition, can be directly attached to the pore walls.[15] Sensors with such molecular recognition elements can be very efficient in molecular detection but they are essentially "single use" devices as they are based on strong and irreversible recognition affinities. An alternative recognition element is a chelator, such as the nitrilotriacetic acid (NTA) group, which in complex with a nickel ion enables specific binding of a polyhistidine (His) tagged protein. Wei et al, for example, developed a gold-modified nanopore functionalized with HS–$(CH_2)_{15}$–$(OC_2H_4)_3$–NTA, and these pores showed a strong increase of the dwell time for His-tagged proteins.[8b] Various NTA-based methods have also been used on planar or macroporous surfaces for protein immobilization (*e.g.* ref. [16]). Recent studies on functionalization of silicon-based and polymeric nanopores with metal-organic chelates emphasized the need for reversible functionalization inside nanopores.[17]

The new strategy for selective and reversible immobilization of proteins that we report here is partly motivated by current efforts to reconstitute the selective permeability of the

nuclear pore complex (NPC) in solid state nanopores.[18] NPCs form ~40 nm wide channels in the nuclear membrane and control the exchange of proteins and nucleic acids into and out of the nucleus of eukaryotic cells. Crucial to this function are intrinsically disordered and thus flexible protein domains rich in phenylalanine-glycine dipeptide motifs (nucleoporin FG domains),[19] which are grafted at high density to the NPC channel wall and efficiently preclude the passage of large inert macromolecules. Such macromolecules can, however, efficiently permeate when bound to soluble nuclear transport receptors (NTRs) that engage in low-affinity interactions with FG domains. Given the broad interest in this system, we mostly use an FG domain (from the yeast nucleoporin Nsp1) as a model protein to analyse the quality and features of our surface functionalization strategy. The strategy itself, however, is generic and can be applied to other His-tagged proteins.

In this paper, we establish a protein coating approach for silica-based surfaces of arbitrary geometry that enables stable and selective immobilization of proteins with controlled orientation and tunable surface density. For attachment to the surface, we use site-specific polyhistidine (His) tags in recombinant proteins. Contrary to the common strategies for anchoring proteins, the capture of proteins *via* the His tag is reversible and proteins can be put on and off, which can be monitored in real time in experiments on planar surfaces and individual nanopores. More specifically, whilst FG domain immobilization to nanopore walls in previous studies was covalent, exploiting the binding of cysteines either directly to gold coated membranes[18a] or to chemically modified SiN,[18b] the method developed here permits the binding of His-tagged proteins in a stable and oriented manner. Importantly, their triggered release enables reversible functionalization, and single nanopores can thus be used for several successive experiments.[16d, 17b, 20] The method can be applied on all silica-based surfaces, such as silica wafers, silicon nitride, or glass, which present a surface that is chemically equivalent to silicon oxide.

As a Ni^{2+} chelator for His tag capture, we use ethylenediaminetetraacetic acid (EDTA) mono amide which has two major advantages over the traditional NTA group. First, its introduction into silica surfaces requires only bulk chemicals (an aminosilane, EDTA and a water-soluble carbodiimide) and follows a simpler chemistry.[21] Second, it provides 6 instead of 4 coordination sites and therefore binds Ni^{2+} far stronger than an NTA group. EDTA mono amide is therefore highly resistant against Ni^{2+} leakage or reduction, even in the presence of free chelators or DTT.[21a]

In this study, we first present the surface functionalization method and characterize its performance in terms of model protein immobilization on planar surfaces with quartz crystal microbalance (QCM-D) and spectroscopic ellipsometry (SE). Then, the versatility of the method is demonstrated by three application examples:

i. The analysis of molecular interactions and protein film morphologies on planar surfaces.
ii. The combination of the His-tag capturing function on silica with passivation for the selective chemical modification of dual gold /silica-based substrates, which are suitable candidates for the fabrication of selective functional patterned platforms or three-dimensional topographic structures[7b, 9] required for advanced biosensing and sieving applications[22] and nanoporous plasmonic sensors.[23]
iii. The implementation of the functionalization method to the more complex topology of SiN nanopores, where we monitor the reversible immobilization of model proteins and the reuse of nanopores *in situ* through ion current measurements.

2. Results and discussion

2.1. Functionalization of silicon oxide surfaces for selective, oriented, and reversible immobilization of His-tagged proteins

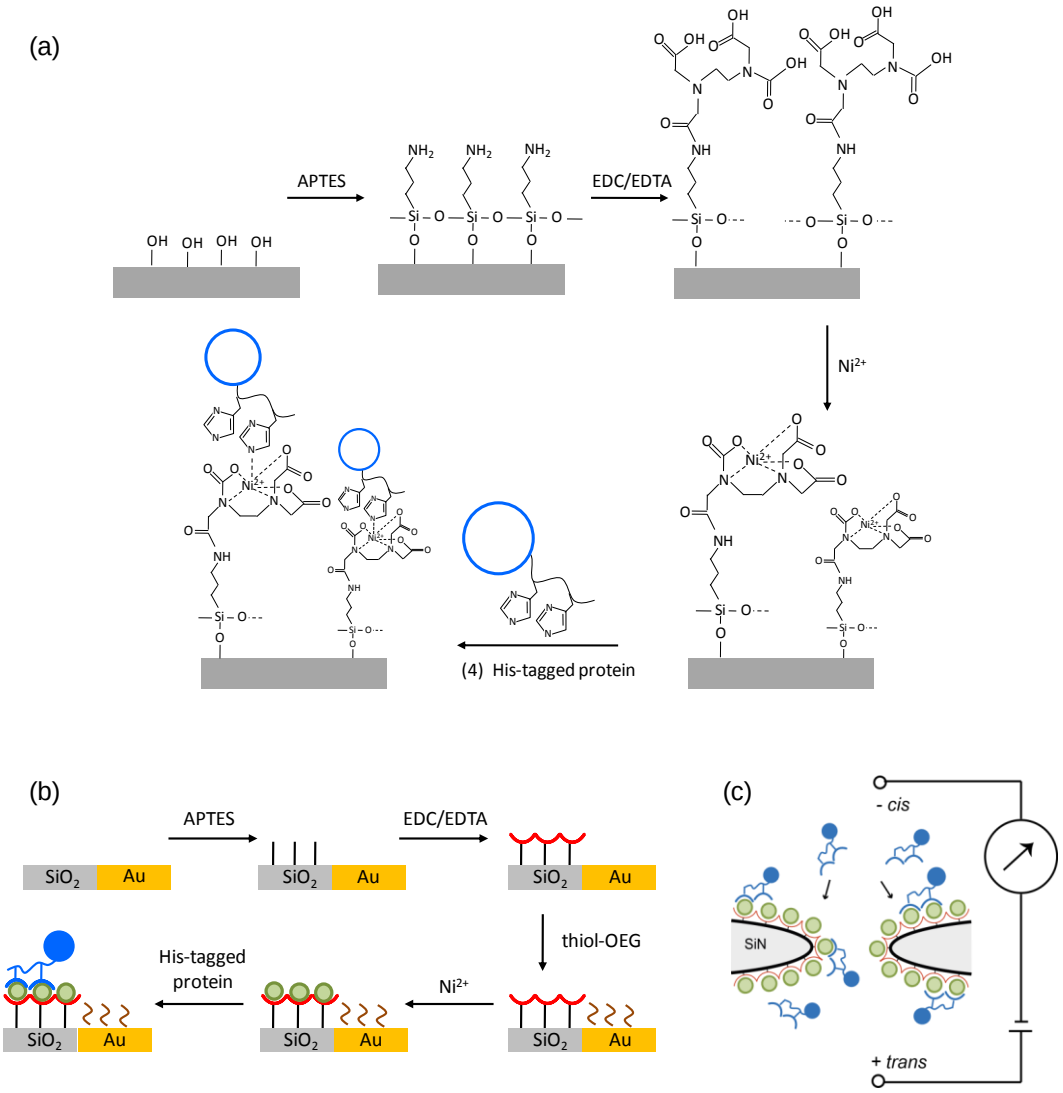

Figure 1. Functionalization of planar surfaces and nanopores. (a) Schematic representation of the surface functionalization method for specific immobilization of His-tagged proteins on silica-based surfaces. (b) Schematic representation of the orthogonal functionalization of silica (for specific immobilization of His-tagged proteins, as in (a)) and gold (for passivation against protein adsorption). (c) Schematic representation of a functionalized nanopore (as in (a)) for immobilization of His-tagged proteins and conductance measurements to monitor ion fluxes through the pore. Stable immobilization of His-tagged proteins is thought to require multivalent attachment, illustrated in (b) and (c) as anchorage to two EDTA moieties.

The functionalization of silicon oxide surfaces contained two sequential chemical conjugation steps: surface OH groups first reacted with the aminosilane APTES, and subsequently EDTA was coupled to the resulting dense layer of primary amines **(Figure1**a). The EDTA mono amide (EDTA for short in the following) thus generated was used to chelate nickel ions which can specifically coordinate with histidine moieties and thus enable the selective and oriented immobilization of His-tagged proteins.

Quartz crystal microbalance with dissipation monitoring (QCM-D) was used to monitor protein binding and assess the quality of immobilization (**Figure2**a). Strong shifts in resonance frequency, Δf, and dissipation, ΔD, were achieved upon incubation of the model protein Nsp1-H_{10}, demonstrating the formation of a soft and hydrated film of this nucleoporin FG domain. The proteins remained stably bound upon rinsing in buffer (typically > 90% were retained over rinsing periods of 30 min) but could be fully released by incubation with 500 mM imidazole (for at least 20 min; longer times had no additional effect) which competes with the His tag for the coordination of the nickel ions. Moreover, an equivalent protein construct that lacked the His tag hardly bound to the Ni^{2+}-EDTA functionalized surfaces (**Figure S1**). These results demonstrate that the proteins bind exclusively *via* their His tag, thus enabling immobilization in a well-defined orientation through a specifically tailored site (here the C terminus) on the protein. The affinity of individual interactions between an EDTA-coordinated Ni^{2+} and a histidine is expected to be of rather low affinity. The high stability of Nsp1-H_{10} against elution in buffer thus indicates that anchorage is realized through multiple histidine-Ni^{2+}-EDTA complexes.

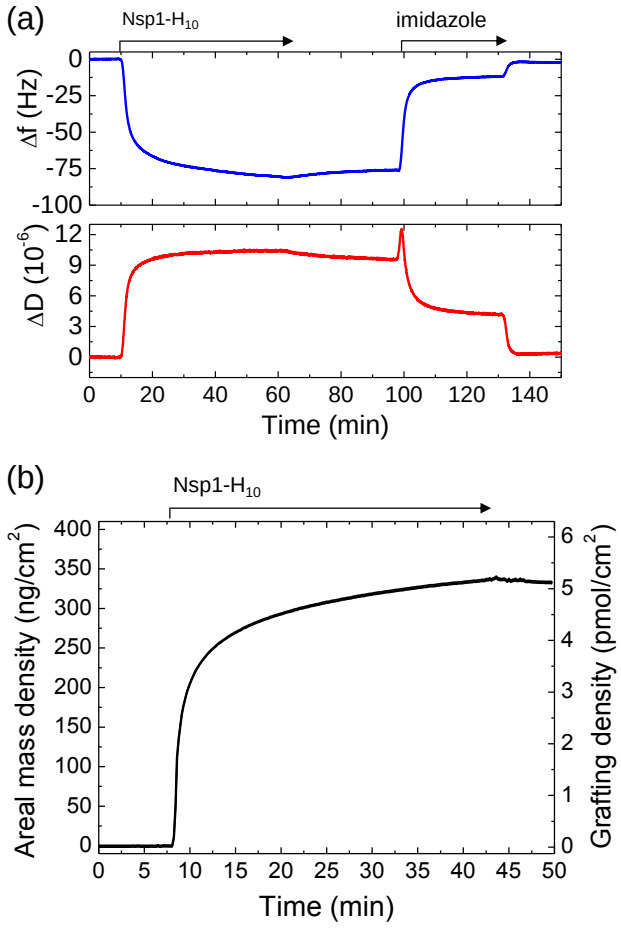

Figure 2. Characterization and quantification of the immobilization of His-tagged proteins on planar silica surfaces. (a) Immobilization of Nsp1 with a C-terminal His tag (Nsp1-H_{10}), and triggered release with imidazole, monitored by QCM-D. Arrows on top of the graph indicate the start and duration of incubation with different sample solutions; remaining times correspond to rinsing with working buffer. Changes in Δf and ΔD upon exchange from imidazole-containing solution to buffer do not reflect any changes on the surface but result from a change in the viscosity and density of the surrounding solution owing to the presence of imidazole. (b) Areal surface densities upon immobilization of Nsp1-H_{10} quantified by SE. Conditions: buffer – 10 mM HEPES, 150 mM NaCl, pH 7.4; Nsp1-H_{10} – 1.5 μM; imidazole – 0.5 M; silica surfaces were functionalized with EDTA and loaded with $NiCl_2$ (2 mM, 15 min) prior to the measurements.

The protein surface density was quantified by spectroscopic ellipsometry (SE). A surface density of 5 pmol/cm^2 (320 ng/cm^2) was easily reached with the typical incubation conditions (Figure 2b). This density corresponds to a root-mean-square distance between

anchor points of approximately 6 nm, comparable to the size of proteins (*e.g.* streptavidin has dimensions around 5 nm at a molecular mass of 60 kDa) and illustrating that a dense protein coating can readily be achieved. Lower film densities can be produced by adjusting the concentration and time of protein incubation, and quantitatively controlled thanks to the kinetic information which is also provided by SE (Figure 2b). The surfaces showed a good batch-to-batch reproducibility in protein binding (**Figure S2**). Moreover, functionalized SiN substrates performed similar to functionalized silica wafers (Figure S2). Both types of substrate are expected to be covered with a thin film of silicon oxide, and indeed they appeared chemically identical for the purpose of the here-presented surface modification.

The SE data in **Figure3**a demonstrate that the functional surfaces can be regenerated and re-used multiple times without an appreciable loss in activity. Across three successive Nsp1-H_{10} incubations on the same surface, the areal protein mass densities reached after 30 min of exposure agreed to well within 5% (337 ± 8 ng/cm^2). We also found the surfaces to remain functional upon repeated wetting with aqueous solution and subsequent drying. Figure 3b evaluates the performance of two sensors that were used many times and stored in air at room temperature between measurements. In this plot, the efficiency of protein immobilization is quantified by the QCM-D frequency shift reached after 1 h of Nsp1-H_{10} incubation relative to the response obtained during the first incubation of Nsp1-H_{10} right after surface functionalization (day 0) under otherwise identical conditions. This parameter is a measure of the relative changes in areal protein mass density. The data show that the His-tag binding capacity is retained at a level above 70% during the first month (comprising 6 uses) and remains above 60% after 3.5 months (9 uses). This demonstrates that the surfaces also retain very good activity when stored over several months.

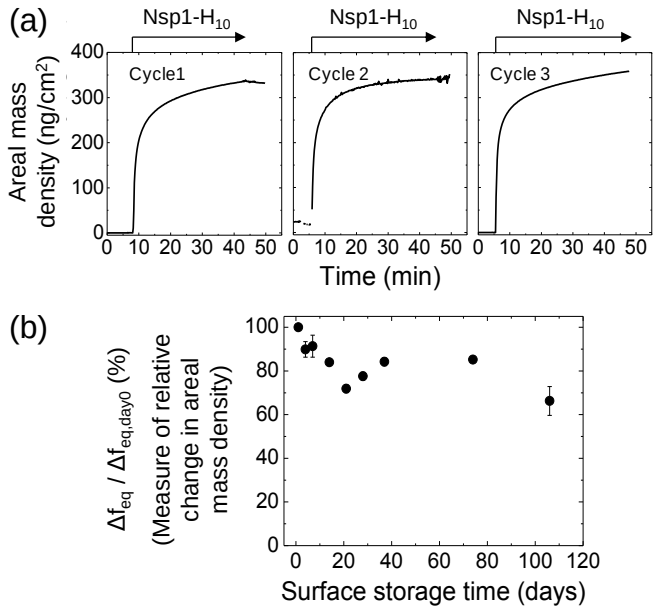

Figure 3. Multiple use of His-tag capturing surfaces, and stability upon storage. (a) Three cycles of Nsp1-H_{10} immobilization on the same surface monitored by SE. The second cycle was performed immediately after the first, and the third cycle one week later; surface regeneration steps are not shown, yet the quality of surface regeneration is reflected by the proximity to zero of the baseline prior to the subsequent protein injections. Conditions: buffer – 10 mM HEPES, 150 mM NaCl, pH 7.4; Nsp1-H_{10}– 1.9 μM; the silica surface was functionalized with EDTA, and after each incubation cycle, the surface was regenerated with a solution of 0.5 M imidazole and 1 M GuHCl (for 40 min, not shown); the surface was loaded with $NiCl_2$ (2 mM for 15 min) prior to each protein incubation step. (b) QCM-D frequency shifts upon incubation with Nsp1-H_{10} (1.5 μM for 60 min) are shown as a function of storage time relative to the response at day 0; the parameter $\Delta f_{eq}/\Delta f_{eq,\ day\ 0}$ is an approximate measure of the changes in areal mass density relative to day 0, and reflects the conservation of His-tag binding capacity. Before each measurement, the surfaces were re-loaded with $NiCl_2$; after each measurement, the surfaces were regenerated with 0.5 M imidazole and 1 M GuHCl (30 min), rinsed with buffer and water, blow-dried in nitrogen gas and stored dry in the dark at room temperature until the next measurement. Error bars represent standard deviations for two measurements with two different sensors; the same sensors were repeatedly used to acquire all data shown in (b).

2.2. Application example I. Analysis of molecular interactions and protein film morphology on planar surfaces

To illustrate the versatility of the Ni^{2+}-EDTA functionalized surface for protein immobilization, we analyzed the binding of three different His-tagged proteins with distinct structural properties (**Figure4**a). Next to the wild type form of the FG domain of Nsp1 (Nsp1-H_{10}), we used a mutant form (Nsp1-H_{10} FILV→S) of identical size in which all hydrophobic amino acids where replaced by serines.[19d] Nsp1 and Nsp1 FILV→S are both intrinsically disordered, but the mutant exhibits a reduced inter- and intra-chain attraction (cohesiveness) compared to the wild type Nsp1.[19a] We have previously shown that the reduced cohesiveness affects the morphology of one-end grafted FG domains considerably, leading to less dense and softer films.[19d] Finally, we also used green fluorescent protein with an N-terminal His tag (H_{14}-GFP) as an example of a 'conventional' folded, globular protein.

Figure 4a-b demonstrates that all three proteins can be stably immobilized, and also almost fully released with 0.5 M imidazole confirming specific and oriented binding *via* the His tag. Moreover, the effective surface regeneration achieved by the imidazole rinse (typically to within 10% of the total protein binding, *cf.* Figs. 2a, 3a, 4a-b and S2b) enabled sequential studies with the different proteins on the same sensor surface.

Planar surfaces enable characterization of proteins and protein films with surface sensitive techniques at a level of detail that is difficult to achieve on more complex surface geometries. This makes them attractive as tools to study biomolecular interactions and self organization. Moreover, it also makes them ideal to tailor and quality control surface functionalization and protein immobilization methods prior to their application on more complex surface geometries. To illustrate both aspects, we here briefly compare the QCM-D responses for the three proteins on Ni^{2+}-EDTA functionalized surfaces with each other, and

with earlier works where we had used another functionalization platform – supported lipid bilayers with nickel-loaded nitrilotriacetic acid (Ni^{2+}-NTA SLBs) – for anchorage of the same proteins.[19d, 24] The Ni^{2+}-NTA SLB platform, as the Ni^{2+}-EDTA surfaces, provides for the selective and reversible binding of His-tagged proteins. Differences are that the SLBs retain the protein anchors laterally mobile and that they are not stable upon drying, which limits their use in certain sensor applications.

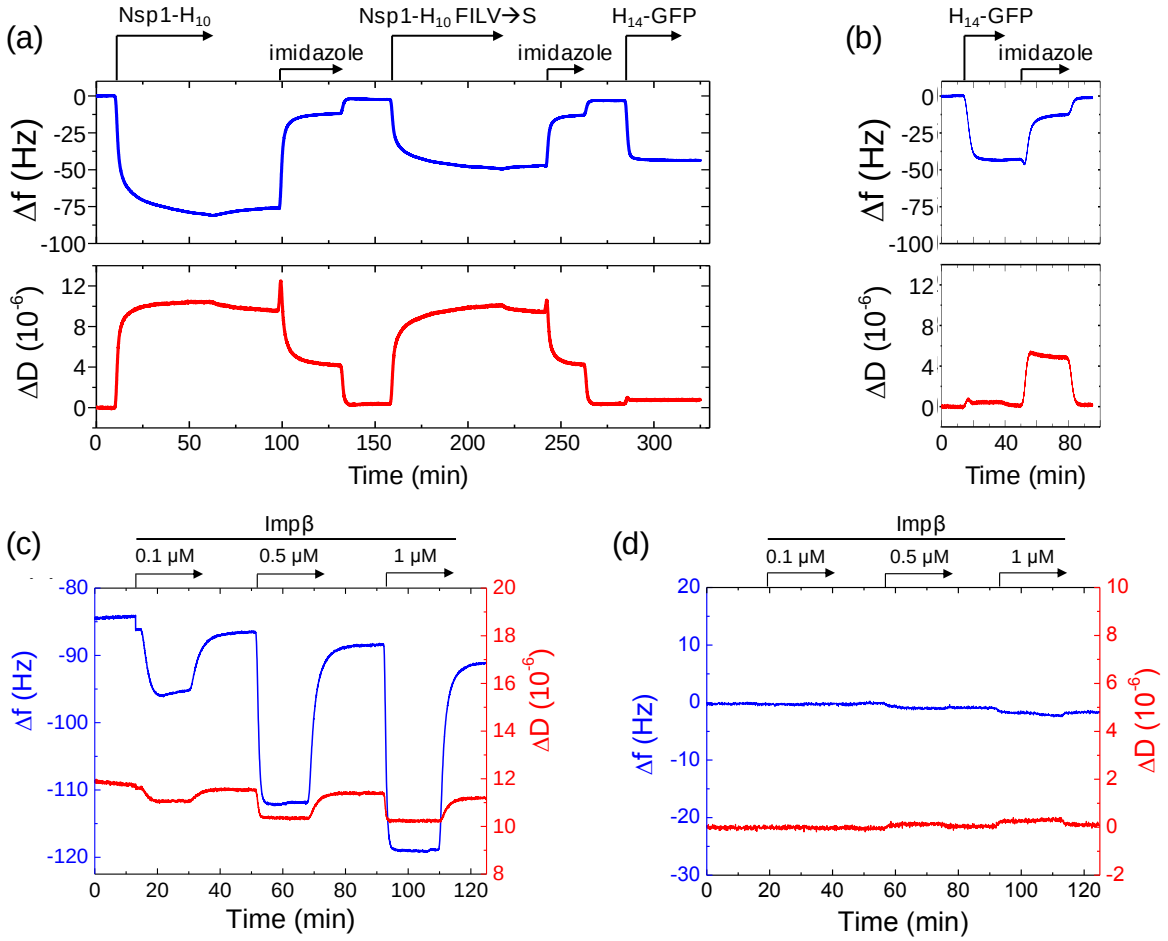

Figure 4. Versatile use of the His-tag capturing surface and selective protein-protein interactions, studied by QCM-D. (a) Consecutive immobilization of three different His-tagged proteins – Nsp1-H_{10}, a FILV→S mutant of Nsp1-H_{10}, and H_{14}-GFP. Conditions: buffer – 10 mM HEPES, 150 mM NaCl, pH 7.4; all proteins – 1.5 μM; between incubation cycles, proteins were released and the surface was thus regenerated by 0.5 M imidazole (as shown). Data are presented analogous to Fig. 2a. (b) Immobilization of H_{14}-GFP to a virgin His-tag capturing surface, and triggered release (conditions as in (a)). (c) The nuclear transport receptor

Impβ reversibly binds to a film of immobilized Nsp1-H_{10} in a dose-dependent manner (decrease in Δf) and rigidifies the Nsp1 film (decrease in ΔD). (d) In the absence of Nsp1-H_{10}, there is only minor Impβ binding, confirming that Impβ binding to the Nsp1-H_{10} film is specific. Conditions: buffer – 10 mM HEPES, 150 mM NaCl, pH 7.4. Silica surfaces were functionalized with EDTA and loaded with $NiCl_2$ (2 mM for 15 min) prior to the measurements in (a) to (d); in addition, an Nsp1-H_{10} film was formed in (c), as shown in Figure 2a.

The QCM-D responses in Figure 4a reveal characteristic differences in the morphology of the protein films that mirror the structural features of the proteins. The frequency shift for H_{14}-GFP at saturation (Δf = -40 Hz) corresponds to a film thickness of approximately 6 nm [25] which is consistent with the size of the protein, while the small dissipation shift ($\Delta D = 0.6 \times 10^{-6}$) reflects the globular (and thus rigid) nature of the protein. The two Nsp1 constructs generate a much higher dissipation, reflecting the formation of soft films. A detailed analysis of the $\Delta D / -\Delta f$ ratio, which is a measure of the elastic compliance of thin films,[25] reveals that the FILV→S mutant forms softer films than the wild type protein, as expected given its reduced cohesiveness (**Figure S3**). Moreover, Figure S3 also shows a gradual rigidification of the Nsp1 films as the protein surface coverage increases. The one-end grafted Nsp1 forms a continuous film of flexible, interpenetrating protein chains (also called 'brush') and the rigidification is the expected consequence of an increase in film density with surface coverage.[19d, 24] Notably, all these observations are consistent with previous studies in which the same three proteins had been anchored to Ni^{2+}-NTA SLBs[19d, 24] instead of Ni^{2+}-EDTA surfaces (see Figure S3), demonstrating that the morphology of the protein films is similar and independent of the exact surface chemistry used for His-tag anchorage.

Comparison of Figure 4a-b with the previous work also shows that the kinetics of protein binding on the Ni^{2+}-EDTA surfaces is comparable to the Ni^{2+}-NTA SLBs. Binding is limited by mass transport at low coverages but steric constraints slow down the binding as the

surface is increasingly populated with proteins. Here, the packing constraints of the globular H_{14}-GFP are relatively weak and the equilibrium state of a dense protein monolayer is reached rather rapidly (within 10 min; on Ni^{2+}-EDTA surfaces, Fig. 4a-b, and on Ni^{2+}-NTA SLBs, Fig. 2 in ref. [24]). The barrier to binding imposed by the film of interpenetrating Nsp1 chains is more severe, particularly so for the less cohesive FILV→S mutant,[19d] and as a consequence, binding of the Nsp1 constructs does not saturate over 1 h of protein incubation. It is notable that the maximal frequency shifts obtained for H_{14}-GFP on Ni^{2+}-EDTA (Figure 4a) and on Ni^{2+}-NTA SLBs (ref. [24]) were identical, confirming formation of a dense protein monolayer. For Nsp1-H_{10} and Nsp1-H_{10} FILV→S, the final frequency shifts were somewhat lower (20 to 30%) on Ni^{2+}-EDTA than on Ni^{2+}-NTA SLBs.[19d] The reason for this difference is not entirely clear, but it suggests that the density of His-tag immobilization sites on Ni^{2+}-EDTA is somewhat smaller than what can be attained on Ni^{2+}-NTA SLBs. It appears also possible that the lateral mobility of the anchoring points on the SLBs facilitates local rearrangements and thus protein binding.

Figure 4c-d illustrates the application of Ni^{2+}-EDTA functionalized surfaces for biomolecular interaction studies. Specifically, we measured the selective interaction between a nuclear transport receptor (NTR) and an FG domain film. Interaction between NTRs and FG domains are known to be essential for the facilitated permeation of large macromolecules through nuclear pore complexes (NPCs). Here, we selected importin β (Impβ) from yeast as the NTR to interact with the Nsp1-H_{10} FG domain. Titration measurements by QCM-D demonstrated Impβ binding to Nsp1 films in a dose-dependent manner (Figure 4c). A control on bare Ni^{2+}-EDTA surfaces (Figure 4d) showed no appreciable Impβ binding, confirming that genuine Impβ-Nsp1 interactions are being probed. Binding and unbinding of Impβ was rapid, indicating fast and reversible interactions with Nsp1. It is notable that the shifts in dissipation upon Impβ binding are negative though generally small relative to the total dissipation shift of

the Nsp1 film. These observations are again consistent with previous reports for Nsp1-H_{10} brushes on Ni^{2+}-NTA SLBs.[19b, 19c] Following the detailed analysis in ref. [19b], we can conclude from the frequency and dissipation data that NTR binding promotes a minor increase in film thickness and a moderate increase in film rigidity whereas the data is inconsistent with an NTR-induced film collapse. Taken together, these examples demonstrate that the developed planar His-tag capturing surfaces are versatile to study interactions between biomolecules in general, and between FG domains and NTRs in particular.

2.3. Application example II. Orthogonal functionalization of silica and gold surfaces

Sensing techniques increasingly rely on the use of structured surfaces that exhibit chemical (next to topographical) contrast on the nanometer or micrometer scale, or on the use of fluidic devices that expose the sample fluid to surfaces with various chemistries. The presence of multiple surface chemistries in one device entails the need to develop methods for selective functionalization of one or another surface. Gold in particular is commonly used in sensors, because it is stable as an electrode in aqueous solution and also of interest for surface plasmon resonance (SPR) sensing. Silicon-based materials are also very attractive because of their optical transparency (quartz or borosilicate glass) and their versatile use in the semiconductor industry (silicon wafers). Here we combine orthogonal silane and thiol chemistries to functionalize silica and gold surfaces such that His-tagged proteins are selectively immobilized on silica while the gold remains inert to protein binding.

The method builds on the APTES/EDTA functionalization of silica (Figure 1a) but includes the deposition of thiol-terminated oligo(ethylene glycol) (thiol-OEG) on gold as an additional step prior to nickel loading (Figure 1b). The quality and orthogonality of the functionalization steps was evaluated by QCM-D using sets of two sensors, one coated with silica and the other with gold, that were jointly exposed to the full set of incubation steps

outlined in Figure 1b. Nsp1-H$_{10}$ again served as a model protein. **Figure 5** shows QCM-D responses upon protein incubation and triggered release on silica that were comparable to those obtained previously (Figure 2a), demonstrating that the thiol-OEG incubation step does not affect the quality of the Ni^{2+}-EDTA functionalization.

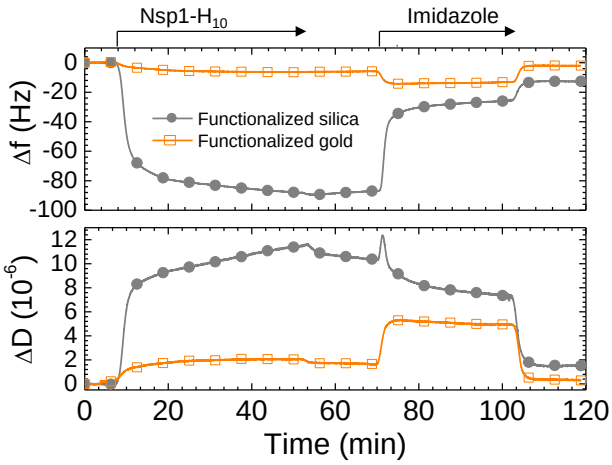

Figure 5. Orthogonal functionalization for selective immobilization of His-tagged proteins to silica surfaces whilst passivating gold surfaces. Binding and triggered release of Nsp1-H$_{10}$, monitored by QCM-D. The magnitudes of the responses on the silica surface (closed symbols) are comparable to data in Figure 2a (demonstrating proper silica functionalization) but much lower on the gold surface (open symbols; indicating effective – yet imperfect – passivation of gold). The over-proportional change in ΔD compared to Δf on gold reflects that residual Nsp1 adsorbs as a rather soft film. Conditions: buffer – 10 mM HEPES, 150 mM NaCl, pH 7.4; Nsp1-H$_{10}$ – 1.5 μM; imidazole – 0.5 M; prior to the measurement, silica and gold surfaces were exposed together to the functionalization steps outlined in Figure 1b.

At the same time, protein binding to gold induced a 90% smaller frequency shift than on silica (Figure 5), and also a 90% smaller frequency shift than on bare gold and on gold that had been exposed to APTES and EDTA but not to thiol-OEG (**Figure S4**), indicating effective passivation of the gold surface. We also tested gold that had been exposed to thiol-OEG (but not to APTES or EDTA), and found no detectable binding of Nsp1-H$_{10}$ (Figure S4). The residual binding to gold treated with orthogonal functionalization (Figure 5) thus indicates that

the APTES and/or EDTA conjugation steps perturb the formation of the thiol-OEG layer, although to a minor degree. It is notable that the residually bound Nsp1-H_{10} can be fully released with imidazole, indicating that protein binds to the gold through the His tag. This suggests that a residue of EDTA is retained on the gold surface even after thiol-OEG deposition. Binding of APTES to gold has previously been reported,[22b, 26] and it might be that this also entails the retention of EDTA. We found that the surfaces exposed to orthogonal functionalization also showed good retention of their activity during repeated use over the course of at least one month (**Figure S5**).

2.4. Application example III. *In-situ* reversible protein attachment to solid-state nanopores

To evaluate the applicability of the Ni^{2+}-EDTA functionalization on more complex surface geometries, we tested its performance with solid-state nanopores (Figure 1c). The procedure for functionalizing SiN membranes (20 nm thickness) containing a single nanopore (approximately 45 nm diameter) was identical to what we established above on planar surfaces, and was performed *ex situ*. The process of protein grafting on the inner surface of the pore was, however, subsequently done *in situ*. To this end, the nanopore was mounted into a custom-made flow cell for measurements of the ion current. The channels of the flow cell were flushed with working buffer, and care was taken to keep the membrane wet throughout the measurement. Current *versus* voltage (*I*/*V*) curves were recorded from -200 mV to +200 mV to test the quality of the pore. A minority of the tested Ni^{2+}-EDTA functionalized pores (6 out of 17) were found to be either asymmetric in the *I*/*V* characteristics (indicating an asymmetric pore or functionalization), or to have increased conductance (indicating pore growth) or very low conductance (indicating clogging by the multi-step chemical treatment). By contrast, most pores (11 out of 17) yielded the expected conductance level of marginally less than bare pores

(95 ± 4 %, mean ± s.d.) at the given measurement conditions, and these pores were used for protein-binding studies.

After setting up the experiment, the baseline current across the nanopore was recorded at -100 mV. The model protein Nsp1-H_{10} was then flushed into the *cis* chamber of the nanopore assembly (cf. Figure 1c) while the current was continuously monitored. **Figure6**a shows a gradual decrease in the conductance during protein exposure (1 to 7 min) starting from the baseline level (75 nS) until a new equilibrium is reached at 24 nS. This lowering of the conductance is consistent with the formation of a film of Nsp1-H_{10} proteins that are anchored at the nanopore walls and enhance the pore resistance. The binding of Nsp1-H_{10} is specific to the Ni^{2+}-EDTA functionalization: no significant changes in conductance were observed when bare SiN pores were exposed to Nsp1-H_{10} constructs (**Figure S6**).

Comparative transmission electron microscopy of the nanopore before and after coating with Nsp1-H_{10} (**Figure S7**) provided further evidence for protein attachment. Next, the nanopore was subjected to a regeneration protocol, which consisted of incubation with a regeneration mixture (1 M imidazole and 1 M GuHCl; 20 min) followed by washing with ultrapure water, then a 1:1 (*v*/*v*) mixture of ethanol and water, and finally with measurement buffer to complete one cycle. This led to a recovery of the conductance to a level of 67 nS, *i.e.*, close to the starting conductance value.

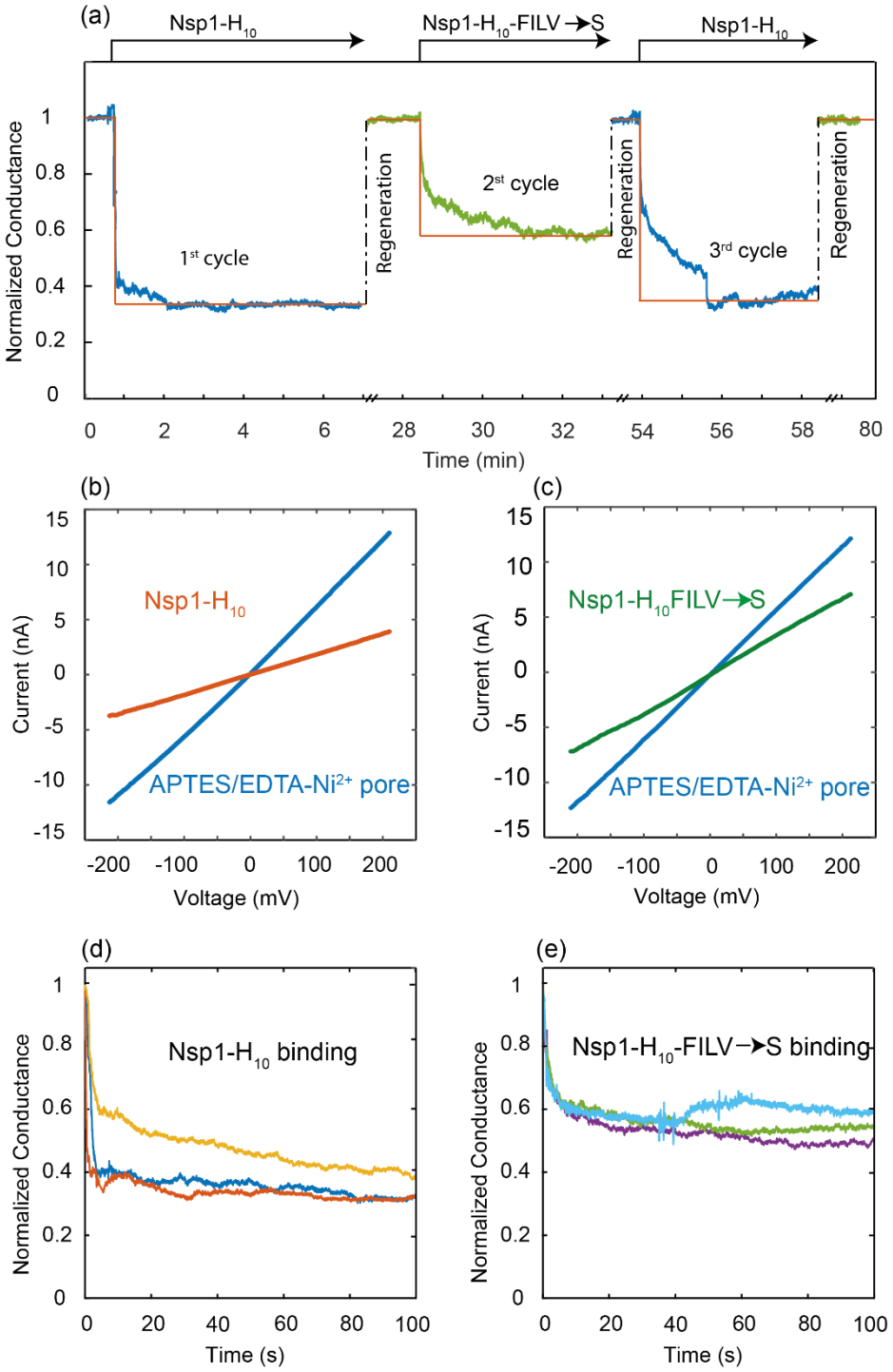

Figure 6. Real time monitoring of protein immobilization in solid-state nanopores. (a) Ion current *I*, continuously recorded at an applied voltage *V* = -100 mV across a Ni^{2+}-EDTA-functionalized nanopore of 40 nm diameter, during sequential cycles of protein injection (Nsp1-H_{10} – blue, Nsp1-H_{10} FILV→S – green) and surface regeneration (regeneration steps not shown). The red line is a guide to the eye, and the plotted current traces were low-pass filtered at 1 kHz and down-sampled 100 times. (b-c) Current *vs.* voltage (*I*/*V*) curves for a nanopore functionalized with Ni^{2+}-EDTA (blue), and incubated with Nsp1-H_{10} (red) or Nsp1-

H_{10} FILV→S (green). Data correspond to the first and second cycle in (a). (d-e) Conductance *vs.* time for injection of Nsp1-H_{10} (d) and Nsp1-H_{10} FILV→S (e). Three representative binding curves are shown for each case, and the conductance was normalized by the conductance prior to protein injection to facilitate comparison. Conditions: buffer – 10 mM Tris, 150 mM KCl, pH 7.4; Nsp1-H_{10} and Nsp1-H_{10} FILV→S – 1.5 μM; regeneration – 1 M imidazole and 1 M GuHCl, 20 min. Conductance traces were low-pass filtered at 1 kHz and down sampled 100 times.

To assess the possibility of reusing the same pore, we performed additional cycles of protein incubation and pore regeneration. The representative data in Figure 6a (>28 min) shows clear conductance shifts for both Nsp1-H_{10} FILV→S (2^{nd} cycle) and Nsp1-H_{10} (3^{rd} cycle), indicating successful immobilization of the protein and regeneration of the pore. The *I*/*V* curves after coating the pore with proteins were found to be linear (Figure 6b-c, red and green traces). The pores filled with protein thus retain the ohmic behaviour of the bare Ni^{2+}-EDTA functionalized pores (Figure 6b-c, blue traces), as expected, although the slope of the *I*/*V* curves is smaller due to the reduced conductance with the proteins. Notably, the effect of the FILV→S mutant on the conductance was significantly smaller than that of wild type Nsp1, which is understood from the different organization of these mutant FG domains in the pore.[18c] The protein attachment and regeneration cycles were performed on different pores (n = 3; average size 45 ± 4 nm as measured by transmission electron microscopy; Figure S7) and the conductance dropped from 65 ± 7 nS to 21 ± 4 nS (by 67 %) upon attachment of Nsp1-H_{10}, and from 65 ± 7 nS to 35 ± 6 nS (by 46 %) for Nsp1-H_{10} FILV→S. These conductance values are in good agreement with our previous work on the same proteins, which showed 80% and 50% conductance blockage for Nsp1 and Nsp1 FILV→S, respectively, that were immobilized by cysteine maleimide chemistry.[18c] The Nsp1 FILV→S mutant has a reduced cohesiveness compared to wild type Nsp1, and we have previously shown that this leads to the formation of a less dense biopolymer meshwork[19d] (see also Figure S3). The smaller effect of the FILV→S

mutants on conductivity as compared to wild type Nsp1 reflects an enhanced permeability of monovalent ions and is consistent with a less dense meshwork (see refs. [18c, 27] for the biophysical relevance of the different ion conduction through Nsp1 and Nsp1 FILV→S).

Upon surface regeneration, we regained the baseline conductance level to 93±5 % (n = 4), suggesting that the self-assembled monolayer underneath is retained without damage. The ability to selectively bind and detach proteins at will thus provides the flexibility to tether whichever protein with a polyhistidine tag, in much the same way as we have shown in more detail above for planar surfaces. The used nanopores were later subjected to oxygen plasma treatment, yielding an increase of the pore conductance by 6 ± 3 % (n = 2) compared to the protein-free Ni^{2+}-EDTA functionalized pores. This difference was in agreement with the conductance decrease of 5 ± 4 % (n = 11) observed upon Ni^{2+}-EDTA functionalization.

The time-resolved conductance measurements also shed light on the kinetics of protein binding to the modified nanopore. Close examination (Figure 6d-e) reveals two distinct response regimes upon incubation of the Nsp1 constructs: conductance decreases rapidly during the first seconds of incubation and then more slowly over several minutes before changes become comparable with the noise and a plateau is effectively attained. Similarly, two regimes can also be observed for the binding of the Nsp1 constructs to planar surfaces (by QCM-D and SE, cf. Figures 2, 3a and 4a). We have previously shown that the initial binding of FG domains to planar surfaces is limited by mass transport from the solution, and that a kinetic barrier arises once a continuous polymer film has formed that gradually slows further binding.[19d] Equivalently, two binding regimes would be expected inside the nanopores, and we suggest that this explains the two conductance regimes observed in Figure 6.

3. Conclusions

We have established a surface functionalization method that uses Ni^{2+}-loaded EDTA moieties to selectively immobilize His-tagged proteins on materials that present silicon oxide on their surfaces (such as silicon or silicon nitride wafers and quartz or borosilicate glass) at well-defined orientation and tuneable surface density (Figure 2). The method should be particularly attractive for biosensing applications because the method requires only bulk chemicals and follows a simple chemistry, and the coating can be regenerated and reused multiple times, and retains functionality upon storage for several months (Figure 3). Importantly, the method can be applied to surfaces of complex geometry, as demonstrated here for nanopores (Figure 6). Moreover, the silane chemistry used to form the EDTA coating on silica can be combined with thiol chemistries on gold (here demonstrated with the passivation of gold, Figure 5), making it possible to apply the reversible immobilization of proteins on silica with an orthogonal surface chemistry on gold in the same device.

We demonstrated the benefits of first establishing the surface functionalization on planar surfaces, because these enable detailed, time-resolved and quantitative characterization of protein films (including morphology, surface density, stability of immobilization and triggered release, binding and reorganization processes, and protein-protein interactions; Figures 2-4) with surface sensitive techniques such as QCM-D and SE. The optimized surface functionalization and protein immobilization method was then translated to more complex surfaces such as solid-state membranes with nanopores. Such a two-step approach should also be useful for the establishment of other surface functionalization methods in the context of biosensor development and other applications requiring well-defined surface biofunctionalization.

We have directly demonstrated successful functionalization of nanopores using *in situ* ion current measurements (Figure 6). An attractive target for future efforts will be the functionalization of gold-coated nanoporous SiN membranes, in such a way that His-tagged

proteins are selectively coating the inside of the nanopores (silica) whilst the outer membrane scaffold (gold) remains inert to protein adsorption. This functionalization approach would focus recognition processes to the interior of nanopores. Such functionalization should be useful for advancement in nanopore-based sensing (*e.g.* of biomarkers[28] and antibodies[14]), and also for highly selective filtration and sieving applications.

4. Experimental Section

Functionalization of silicon-based surfaces. (3-aminopropyl)triethoxysilane (APTES), N-(3-dimethylaminopropyl)-N'-ethylcarbodiimide hydrochloride (EDC) and ethylenediaminetetraacetic acid tetrasodium salt hydrate (EDTA) were purchased from Sigma-Aldrich. Four different silicon-based substrates were used: (a) silicon wafers (BT Electronics, Les Ulis, France; for SE measurements), (b) QCM-D sensors with a reactively sputter-coated film of silica (QSX303; Biolin Scientific, Västra Frölunda, Sweden; for QCM-D measurements), (c) Silicon wafers with a 20 nm low-pressure chemical vapour-deposited silicon nitride coating (Dimes Technology Centre, Delft, The Netherlands; for control SE measurements), and (d) silicon nitride membranes (20 nm thickness) with a single nanopore (45 ± 4 nm diameter).[29] Silicon and silicon nitride form a thin layer of 'native' silicon oxide upon exposure to air, and all four surfaces thus effectively present OH groups. Substrates (a) to (c) were cleaned by immersion in an aqueous solution of 2 % sodium dodecyl sulphate (SDS; Carl Roth, Germany; 30 min), followed by rinsing with ultrapure water, ethanol and ultrapure water, blow-drying with nitrogen gas and exposure to UV/ozone (BioForce Nanosciences, Ames, IA; 30 min). Substrate (d) was cleaned by rinsing in ultrapure water, ethanol, acetone and isopropanol followed by gentle blow-drying with nitrogen gas and exposure to oxygen plasma (Pico; Diener Electronic GmbH, Nagold, Germany; 30 s).

Surface functionalization with APTES was performed in the vapour phase, adapting a method previously described by Wang et al.[30] We found this method to reproducibly generate homogeneous silane layers that were stable in aqueous medium, whereas functionalization in the liquid phase may lead to less homogenous and less stable coatings.[31] Specifically, a clean desiccator of approximately 2 L volume was conditioned by purging with argon (5 min), deposition of a drop (30 µL) of APTES, and additional 2 min of argon flow. Freshly cleaned surfaces were then placed inside the desiccator, and following an argon purge for 3 min the desiccator was sealed with parafilm and the sample left to incubate for 1 h. After APTES treatment, samples were sequentially immersed in aqueous solutions containing 0.5 M EDTA and 25 mM EDC at pH 8 (adjusted with HCl) at room temperature, first once for 3 h, then twice for 2 h, and eventually once overnight, rinsed in ultrapure water and blow-dried with nitrogen gas. The solutions were prepared freshly before each incubation step, and the large excess of EDTA over EDC ensured that only one carboxyl group per EDTA reacted with a primary amine on the solid phase.[21a] Prior to use, the EDTA on the solid phase was loaded with nickel ions through immersion in an aqueous solution of 2 mM $NiCl_2$ (15 min).

Functionalization of gold surfaces. A linear oligo(ethylene glycol) derivative containing 7 ethylene glycol units, and with a thiol group on one end and an OH group on the other (thiol-OEG), was obtained from Polypure (Oslo, Norway). QCM-D sensors with a gold coating (QSX301; Biolin Scientific) were used as substrates, and cleaned as the silicon-based surfaces described above. For functionalization, gold surfaces were incubated with 1 mM thiol-OEG in ultrapure water for at least 18 h, rinsed with ultrapure water and blow-dried with nitrogen gas.

Proteins. The main protein used was the FG domain (amino acids 2 to 601) of the yeast nucleoporin Nsp1 with a C-terminal polyhistidine tag (Nsp1-H_{10}; 64.1 kDa). We also used an equivalent mutant construct in which all phenylalanines, isoleucines, leucines and valines were replaced by serines (Nsp1-H_{10} FILV→S; 60.4 kDa), and the wild type Nsp1 FG domain lacking

a histidine tag (Nsp1; 62.1 kDa). FG domain constructs were purified as described earlier[19b] and stored at 10 mg mL^{-1} concentration in 50 mM Tris, pH 8 and 6 M guanidine hydrochloride (GuHCl) at -80°C. Green fluorescent protein with an N-terminal polyhistidine tag (H_{14}-GFP; 27 kDa) was stored at 2.7 mg mL^{-1} concentration in 40 mM Tris, pH 7.5, 260 mM NaCl, 4 mM magnesium acetate, 0.4 mM EDTA, 250 mM saccharose, and 2 mM dithiothreitol at -80°C. The nuclear transport receptor importin β from *Saccharomyces cerevisiae* (Impβ, 95 kDa) was purified as described earlier,[19b] and stored at 9.5 mg mL^{-1} concentration in 40 mM Tris pH 7.5, 260 mM NaCl, 4 mM magnesium acetate, 0.4 mM EDTA, 250 mM saccharose, and 10 mM β-mercaptoethanol at -80 °C. Before use, proteins were diluted in working buffer to desired concentrations; the dilutions of the Nsp1 constructs were chosen such that the residual concentration of GuHCl in the final solutions was below 75 mM.

Buffers. For measurements on planar surfaces, we used a working buffer containing 10 mM HEPES and 150 mM NaCl at pH 7.4. For measurements with nanopores, the working buffer contained 10 mM Tris and 150 mM KCl at pH 7.4. These buffers were chosen according to established routines for the characterization of each substrate; in a comparative QCM-D control measurement on planar surfaces, we verified that Nsp1-H_{10} FILV→S films of comparable surface density and morphology are formed in both buffers (**Figure S8**).

Quartz crystal microbalance with dissipation monitoring (QCM-D). QCM-D monitors changes in resonance frequency Δf and dissipation ΔD of a sensor crystal upon interaction of (soft) matter with its surface. The QCM-D response is sensitive to the mass, including hydrodynamically coupled water, and the mechanical properties of the surface-bound layer.[25] To a first approximation, a decrease in Δf indicates an increase in film areal mass density, and high (low) values of $\Delta D/-\Delta f$ indicate a soft (rigid) film. QCM-D measurements were performed with a Q-Sense E4 system equipped with Flow Modules (Biolin Scientific). The system was operated in flow mode with a flow rate of 10 μL min^{-1} using a syringe pump (KD Scientific,

Holliston, MA, USA), and the working temperature was 23°C. Δf and ΔD were measured with a time resolution of around 1s at the fundamental (i = 1) and six overtones (i = 3, 5, ...,13), corresponding to resonance frequencies $f_i \approx 5, 15, 25, ..., 65$ MHz. Normalized frequency shifts, $\Delta f = \Delta f_i/i$, and dissipations shifts, $\Delta D = \Delta D_i$, for i = 5 are presented; any other overtone would have given qualitatively similar information.

Spectroscopic ellipsometry (SE). SE measures changes in light polarization upon reflection on a sample surface. The ellipsometric angles Δ and Ψ were measured as a function of time and modelled to quantify the surface density of immobilized proteins. A spectroscopic ellipsometer (M2000V; Woollam, Lincoln, NE, USA; wavelength range λ = 380 to 1000 nm) with a horizontal plane of incidence was used, as described in detail elsewhere.[19b, 19c] Briefly, the binding of biomolecules to functionalized silicon wafers was followed in working buffer using a custom-made open-cuvette liquid cell (200 µL volume) with continuously stirred sample solution[19b] at 70° angle of incidence. Sample solutions were injected directly into the buffer-filled cuvette and excess sample was removed by repeatedly diluting the cuvette content in buffer.

Data were fitted with CompleteEASE software (Woollam) using a model of optically homogeneous layers as described in detail in previous work.[19b] Specifically, the SiO_2 (or SiN) layer with APTES/EDTA functionalization, and the protein film, were treated as two distinct transparent Cauchy layers each with an optical thickness h_{SE} and a wavelength-dependent refractive index $n = A + B / \lambda^2$. The surrounding working buffer was also treated as a transparent Cauchy medium with $n_{buffer} = 1.325 + 0.00322 / (\lambda / \mu m)^2$, and the dispersion parameter B of the protein film was assumed to be identical to that of the buffer. Protein surface densities were determined using de Feijter's equation,[32] $\Gamma = h_{SE} \Delta n / (M_w \times dn/dc)$, where Δn is the difference between the refractive indices of the solvated protein film and the surrounding buffer solution,

M_w is the protein molecular weight, and d*n*/d*c* is the refractive index increment (0.18 cm^3g^{-1} for proteins[33]).

Nanopore fabrication and measurements. Nanopores were fabricated on silicon nitride (SiN) membranes deposited on silicon wafers as described elsewhere in detail.[29] In brief, nanopore chips were built-up on a 100 silicon wafer by adding supporting layers of silicon dioxide and low-stress SiN. By employing UV-lithography, reactive-ion etching and chemical etching, these supporting layers were etched away to produce a free-standing SiN window of 10 × 10 μm^2 surface area and 20 nm thickness. A nanopore was drilled into the SiN membrane window by transmission electron microscopy (Tecnai 200STEM-FEG; FEI, Eindhoven, The Netherlands) operated at 300 kV. Membranes with a nanopore were stored in a solution containing 50% (v/v) ethanol in ultrapure water until further use.

For protein immobilization and conductance measurements, a membrane with nanopore was loaded in a custom-made poly(methyl methacrylate) flow cell with 30 µL liquid volume on each side of the membrane (*cis* and *trans*), and the flow cell was flushed with working buffer (at least 3 times the cell's volume). Ag/AgCl electrodes were used to apply electric fields and measure the ionic current across the nanopore. The ionic current was recorded with an electrophysiology patch clamp setup Axopatch 200B amplifier at 100 kHz bandwidth and digitized at 500 KHz (Digidata 1322A DAQ; Molecular Devices, CA, USA). The data was analysed with a custom-made Matlab script.

Acknowledgements

L. Yate (CIC biomaGUNE) is acknowledged for providing metal surface coatings, and A.N.A would like to thank Yaron Caspi for discussions and Diederik Lamen Trip (both Delft University of Technology) for sharing the conductance analysis script. This work was supported by the European Research Council Starting Grant "JELLY" (306435) to R.P.R., the

European Research Council Advanced Grant “SynDiv” (669598) and NanoNextNL (program 07A.05) to C.D., and the Netherlands Organisation for Scientific Research (NWO/OCW) as part of the Frontiers of Nanoscience program.

Author contribution statement

R.P.R. and C.D. conceived the study. All authors contributed to the design of the experiments. D.G. invented the Ni^{2+}-EDTA-amide technology. S.F. and N.E. produced the proteins. M.G., N.A., L.D. and N.E. functionalized the substrates. M.G., N.A., L.D. and N.E. performed experiments on planar surfaces. A.A. performed experiments on nanopores. All authors contributed to the analysis of the data. A.A., M.G., N.A, C.D. and R.P.R wrote the paper.

References

[1] a) F. Traversi, C. Raillon, S. M. Benameur, K. Liu, S. .Khlybov, M. Tosun, D. Krasnozhon, A. Kis, A. Radenovic. *Nat. Nanotechnol.* **2013,** *8*, 939; b) A. P. Ivanov, E. Instuli, C. M. McGilvery, G. Baldwin, D. W. McComb, T. Albrecht, J. B. Edel. *Nano Lett.* **2011,** *11*, 279.

[2] a) C. E. Korman, M. Megens, C. M. Ajo-Franklin, D. A. Horsley. *Langmuir.* **2013,** *29*, 4421; b) C. Duan, A. Majumdar. *Nat. Nanotechnol.* **2010,** *5*, 848; c) C. Ho, R. Qiao, J. B. Heng, A. Chatterjee, R. J. Timp, N. R. Aluru, G. Timp. *Proc. Natl. Acad. Sci. U. S. A.* **2005,** *102*, 10445.

[3] a) M. Pastoriza-Gallego, M.-F. Breton, F. Discala, L. Auvray, J.-M. Betton, J. Pelta. *ACS Nano.* **2014,** *8*, 11350; b) C. C. Striemer, T. R. Gaborski, J. L. McGrath, P. M. Fauchet. *Nature.* **2007,** *445*, 749; c) A. Ivankin, R. Y. Henley, J. Larkin, S. Carson, M. L. Toscano, M. Wanunu. *ACS Nano.* **2014,** *8*, 10774.

[4] Y. Feng, Y. Zhang, C. Ying, D. Wang, C. Du. *Genomics, Proteomics Bioinf.* **2015,** *13*, 4.

[5] a) X. Lin, Q. Yang, L. Ding, B. Su. *ACS Nano.* **2015,** *9*, 11266; b) I. Vlassiouk, P. Y. Apel, S. N. Dmitriev, K. Healy, Z. S. Siwy. *Proc. Natl. Acad. Sci. U. S. A.* **2009,** *106*, 21039.

[6] S. W. Kowalczyk, T. R. Blosser, C. Dekker. *Trends Biotechnol.* **2011,** *29*, 607.

[7] a) K. C. Popat, G. Mor, C. A. Grimes, T. A. Desai. *Langmuir.* **2004,** *20*, 8035; b) M. Pla-Roca, L. Isa, K. Kumar, E. Reimhult. *ACS Appl. Mater. Interfaces.* **2015,** *7*, 6030.

[8] a) M. Wanunu, A. Meller. *Nano Lett.* **2007,** *7*, 1580; b) R. Wei, V. Gatterdam, R. Wieneke, R. Tampe, U. Rant. *Nat. Nanotechnol.* **2012,** *7*, 257.

[9] T. D. Lazzara, T.-T. Kliesch, A. Janshoff, C. Steinem. *ACS Appl. Mater. Interfaces.* **2011,** *3*, 1068.

[10] a) J. Li, D. Stein, C. McMullan, D. Branton, M. J. Aziz, J. A. Golovchenko. *Nature.* **2001,** *412*, 166; b) A. J. Storm, J. H. Chen, X. S. Ling, H. W. Zandbergen, C. Dekker. *Nat. Mater.* **2003,** *2*, 537.

[11] B. M. Venkatesan, R. Bashir. *Nat. Nanotechnol.* **2011,** *6*, 615.

[12] a) M. J. Kim, M. Wanunu, D. C. Bell, A. Meller. *Adv. Mater.* **2006,** *18*, 3149; b) M.-Y. Wu, D. Krapf, M. Zandbergen, H. Zandbergen, P. E. Batson. *Appl. Phys. Lett.* **2005,** *87*, 113106.

[13] R. Wei, D. Pedone, A. Zürner, M. Döblinger, U. Rant. *Small.* **2010,** *6*, 1406.

[14] E. C. Yusko, J. M. Johnson, S. Majd, P. Prangkio, R. C. Rollings, J. Li, J. Yang, M. Mayer. *Nat. Nanotechnol.* **2011,** *6*, 253.

[15] a) V. Mussi, P. Fanzio, L. Repetto, G. Firpo, P. Scaruffi, S. Stigliani, G. P. Tonini, U. Valbusa. *Nanotechnology.* **2010,** *21*, 145102; b) S. M. Iqbal, D. Akin, R. Bashir. *Nat. Nanotechnol.* **2007,** *2*, 243.

[16] a) S. Lata, J. Piehler. *Anal. Chem.* **2005,** *77*, 1096; b) A. Tinazli, J. Tang, R. Valiokas, S. Picuric, S. Lata, J. Piehler, B. Liedberg, R. Tampé. *Chem. Eur. J.* **2005,** *11*, 5249; c) S. Wijeratne, W. Liu, J. Dong, W. Ning, N. D. Ratnayake, K. D. Walker, M. L. Bruening. *ACS Appl. Mater. Interfaces.* **2016,** *8*, 10164; d) T. Muhammad Nawaz, A. Mubarak, A. Rute, M. Werner E. G., S. Heinz-Christoph, T. Wolfgang, E. Wolfgang. *Chem.Commun.* **2013,** *49*, 2210.

[17] a) M. Lepoitevin, M. Bechelany, J.-M. Janot, S. Balme. *Sci. Lett.* **2015,** *4*; b) Z. Chen, T. Chen, X. Sun, B. J. Hinds. *Adv. Funct. Mater.* **2014,** *24*, 4317; c) M. Ali, P. Ramirez, I. Duznovic, S. Nasir, S. Mafe, W. Ensinger. *Colloids Surf., B.* **2017,** *150*, 201.

[18] a) T. Jovanovic-Talisman, J. Tetenbaum-Novatt, A. S. McKenney, A. Zilman, R. Peters, M. P. Rout, B. T. Chait. *Nature.* **2009,** *457*, 1023; b) S. W. Kowalczyk, L. Kapinos, T.

R. Blosser, T. Magalhaes, P. van Nies, R. Y. H. Lim, C. Dekker. *Nat. Nanotechnol.* **2011,** *6*, 433; c) A. N. Ananth, A. Mishra, S. Frey, A. Dwarakasing, R. Versloot, E. v. d. Giessen, D. Görlich, P. Onck, C. Dekker. *Submitted.*

[19] a) S. Frey, R. P. Richter, D. Gorlich. *Science.* **2006,** *314*, 815; b) N. B. Eisele, S. Frey, J. Piehler, D. Gorlich, R. P. Richter. *EMBO Rep.* **2010,** *11*, 366; c) N. B. Eisele, F. I. Andersson, S. Frey, R. P. Richter. *Biomacromolecules.* **2012,** *13*, 2322; d) N. B. Eisele, A. Labokha, S. Frey, D. Gorlich, R. P. Richter. *Biophys. J.* **2013,** *105*, 1860.

[20] a) E. L. Schmid, T. A. Keller, Z. Dienes, H. Vogel. *Anal. Chem.* **1997,** *69*, 1979; b) N. Haddour, S. Cosnier, C. Gondran. *J. Am. Chem. Soc.* **2005,** *127*, 5752.

[21] a) D. Goerlich, S. Frey (imac) *US* 20110071274 A1. **2011**; b) S. Lata, A. Reichel, R. Brock, R. Tampe, J. Piehler. *J. Am. Chem. Soc.* **2005,** *127*, 10205.

[22] a) S. Durán, M. Duch, T. Patiño, A. Torres, O. Penon, R. Gómez-Martínez, L. Barrios, J. Esteve, C. Nogués, L. Pérez-García, J. A. Plaza. *Sens. Actuators, B.* **2015,** *209*, 212; b) E. Briand, V. Humblot, J. Landoulsi, S. Petronis, C.-M. Pradier, B. Kasemo, S. Svedhem. *Langmuir.* **2011,** *27*, 678.

[23] a) M. P. Jonsson, A. B. Dahlin, L. Feuz, S. Petronis, F. Höök. *Anal. Chem.* **2010,** *82*, 2087; b) F. Nicoli, D. Verschueren, M. Klein, C. Dekker, M. P. Jonsson. *Nano Lett.* **2014,** *14*, 6917.

[24] D. Johannsmann, I. Reviakine, R. P. Richter. *Anal. Chem.* **2009,** *81*, 8167.

[25] I. Reviakine, D. Johannsmann, R. P. Richter. *Anal. Chem.* **2011,** *83*, 8838.

[26] D. G. Kurth, T. Bein. *Langmuir.* **1995,** *11*, 3061.

[27] M. Mazzanti, J. O. Bustamante, H. Oberleithner. *Physiol. Rev.* **2001,** *81*, 1.

[28] J. Shim, G. I. Humphreys, B. M. Venkatesan, J. M. Munz, X. Zou, C. Sathe, K. Schulten, F. Kosari, A. M. Nardulli, G. Vasmatzis, R. Bashir. *Sci. Rep.* **2013,** *3*, 1389.

[29] J. A. J. Xander, P. J. Magnus, P. Calin, V. S. Gautam, D. Cees, H. D. Nynke. *Nanotechnology.* **2012,** *23*, 475302.

[30] H. Wang, R. Bash, J. G. Yodh, G. L. Hager, D. Lohr, S. M. Lindsay. *Biophys. J.* **2002,** *83*, 3619.

[31] N. Aissaoui, L. Bergaoui, J. Landoulsi, J.-F. Lambert, S. Boujday. *Langmuir.* **2012,** *28*, 656.

[32] J. A. De Feijter, J. Benjamins, F. A. Veer. *Biopolymers.* **1978,** *17*, 1759.

[33] R. P. Richter, K. B. Rodenhausen, N. B. Eisele, M. Schubert, In *Ellipsometry of Functional Organic Surfaces and Films*, Vol. 52, (Eds: K. Hinrichs, K.-J. Eichhorn), Springer, Berlin, Heidelberg, Germany **2014,** Ch. 11.

Supporting Information

Reversible Immobilization of Proteins in Sensors and Solid-state Nanopores

Adithya Ananth, María Genua*, Nesrine Aissaoui*, Leire Díaz, Nico B. Eisele, Steffen Frey, Cees Dekker[$], Ralf P. Richter[$] and Dirk Görlich*

Supporting Figures

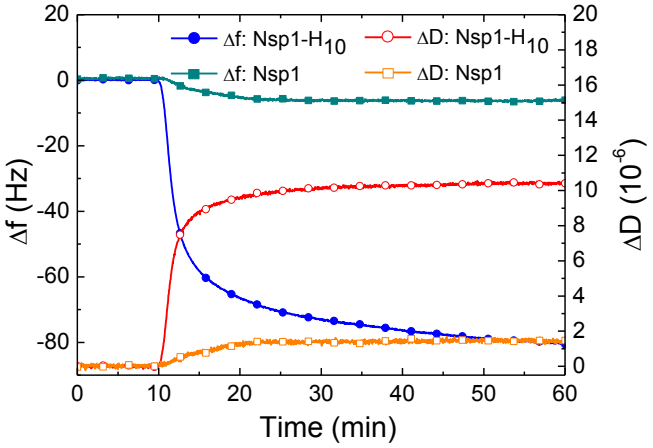

Figure S1. Selectivity for His-tagged proteins. The selective anchoring *via* the His tag was evaluated by comparing the binding of Nsp1-H_{10} with an identical Nsp1 construct that lacks the His tag. While Nsp1-H_{10} binding is comparable to Figure 2, only minor binding is observed for Nsp1. Conditions: buffer – 10 mM HEPES, 150 mM NaCl, pH 7.4; Nsp1-H_{10} and Nsp1 – 1.5µM; surfaces were functionalized with EDTA and loaded with $NiCl_2$ (2 mM for 15 min) prior to the measurements.

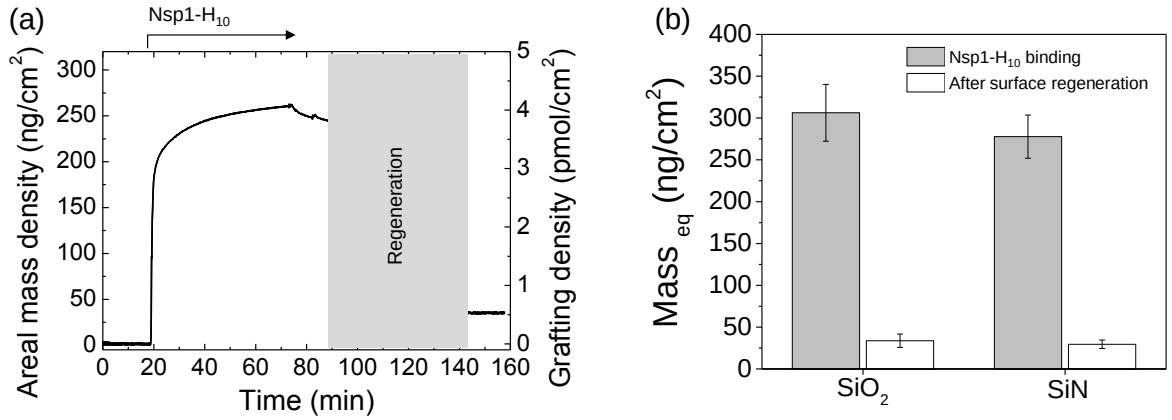

Figure S2. Functional coatings on SiN and SiO_2 have comparable propensity to immobilize His-tagged proteins. (a) SE data of Nsp1-H_{10} binding and triggered release on functionalized SiN with a solution of 0.5 M imidazole and 1 M GuHCl (for 50 min, not shown). The maximal bound amount, binding stability and specificity of binding is comparable to SiO_2 (cf. Figure 2). (b) Averaged areal mass density of immobilized Nsp1-H_{10}, measured by SE after 50 min of incubation at 1.5 µM (grey bars) and after surface regeneration as in (a) (white bars) for functionalized SiO_2 and SiN surfaces. Error bars are standard deviations of independent measurements with 8 different SiO_2 surfaces and 4 different SiN surfaces. Conditions: buffer – 10 mM HEPES, 150 mM NaCl, pH 7.4; Nsp1-H_{10}– 1.5 µM; surfaces were functionalized with EDTA and loaded with $NiCl_2$ (2 mM for 15 min) prior to the measurements.

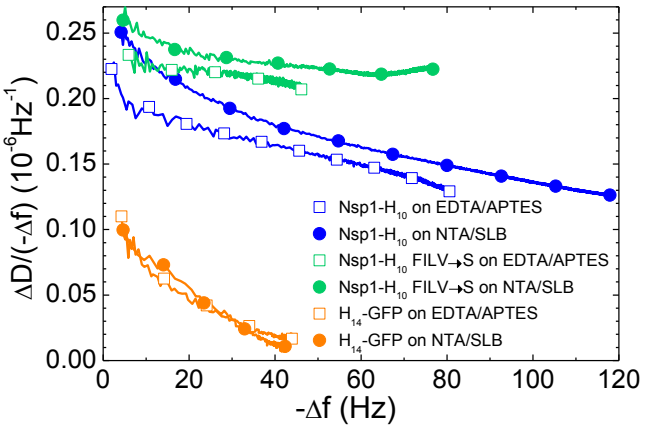

Figure S3. Morphology of protein films. The parameter $\Delta D/-\Delta f$ was derived from QCM-D data and is a measure for the softness of the protein films; $-\Delta f$ is a measure for the surface coverage. Because film mechanical properties and morphology are linked, this parametric plot provides insight into the evolution of the overall film morphology with protein coverage.[24-25] Data for proteins on Ni^{2+}-EDTA on aminosilane are taken from Fig. 4a. For comparison, data on supported lipid bilayers (SLBs) displaying Ni^{2+}-loaded nitrilotriacetic acid (Ni^{2+}-NTA) for capture of His-tagged proteins are also shown (Nsp1-H_{10} and Nsp1-H_{10} FILV→S from Fig. 4 in ref. [19d], H_{14}-GFP from Fig. 2 in ref. [24]). Proteins on aminosilane exhibit the same trends as on SLBs: Nsp1-H_{10} FILV→S films are softer than Nsp1-H_{10} films owing to the reduced cohesiveness of the mutant protein, and both films become more rigid as protein coverage increases and the films become denser. It is notable that Nsp1 FG domain films appear slightly more rigid when formed on aminosilanes as compared to SLBs. We tentatively attribute this to differences in the anchorage: when anchored to the SLBs, proteins are laterally mobile but when anchored to aminosilanes they are not. As expected, the monolayer of globular GFP appears much more rigid than the meshwork of disordered and interpenetrating Nsp1 FG domains. The rigidity of GFP films is comparable on aminosilanes and on SLBs. For GFP, the decrease in $\Delta D/-\Delta f$ with $-\Delta f$ is due to hydrodynamic coupling between proteins, as explained in detail in ref. [24].

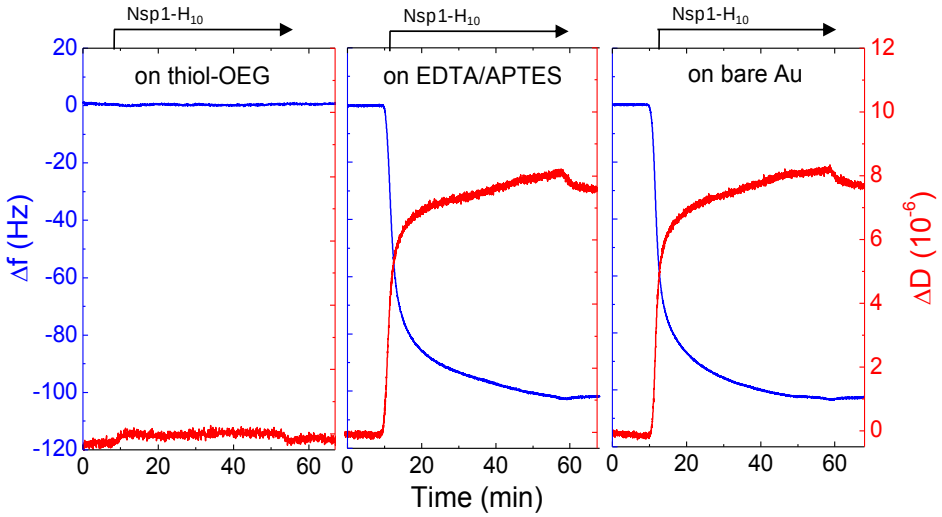

Figure S4. OEG-coated gold surfaces are inert to protein adsorption. The QCM-D shift upon exposure of Nsp1-H_{10} to differently functionalized gold surfaces: thiol-OEG, EDTA/APTES, and bare gold (as indicated). No response is observed on thiol-OEG demonstrating full passivation by comparison to the strong QCM-D shift obtained upon Nsp1-H_{10} adsorption on EDTA/APTES functionalized gold and on bare gold. Conditions: buffer – 10 mM HEPES, 150 mM NaCl, pH 7.4; Nsp1-H_{10} – 1.5 µM.

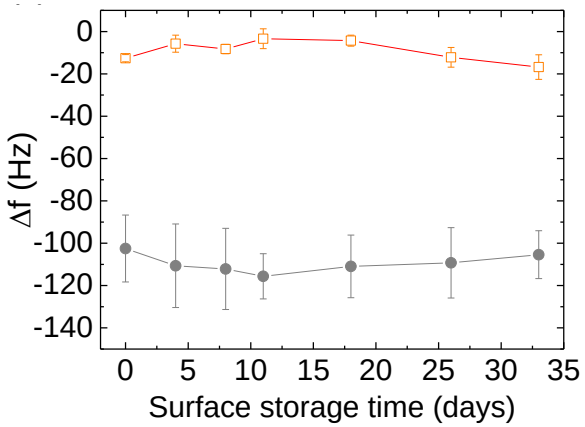

Figure S5. Stability upon storage and re-use of orthogonally functionalized surfaces. QCM-D frequency shifts at equilibrium, upon incubation with a His tagged FG domain H_{18}-Mac98 (0.3 µM for 60 min) are shown as a function of storage time. This reflects the conservation of His-tag binding capacity on silica (grey filled circles) and the passivation of gold (orange open squares) over the course of one month. Before each measurement, the surfaces were re-loaded with $NiCl_2$; after each measurement, the surfaces were regenerated with 0.5 M imidazole and 1 M GuHCl (30 min), rinsed with buffer and water, blow-dried in nitrogen gas and stored dry in the dark at room temperature until the next measurement. Error bars represent standard deviations for two measurements with two different sensors; the same sensors were repeatedly used to acquire all data shown. For this set of measurements, the FG domain of Nup98 from *Tetrahymena thermophila* with an N terminal H_{18} tag (H_{18}-Nup98; 61 kDa; see B. Schmidt, D. Görlich. *eLife.* **2015,** *4*, e04251 for protein preparation) was used thus demonstrating application to another His tagged protein. Additional tests with Nsp1-H_{10} over a period of 20 days showed comparable stability.

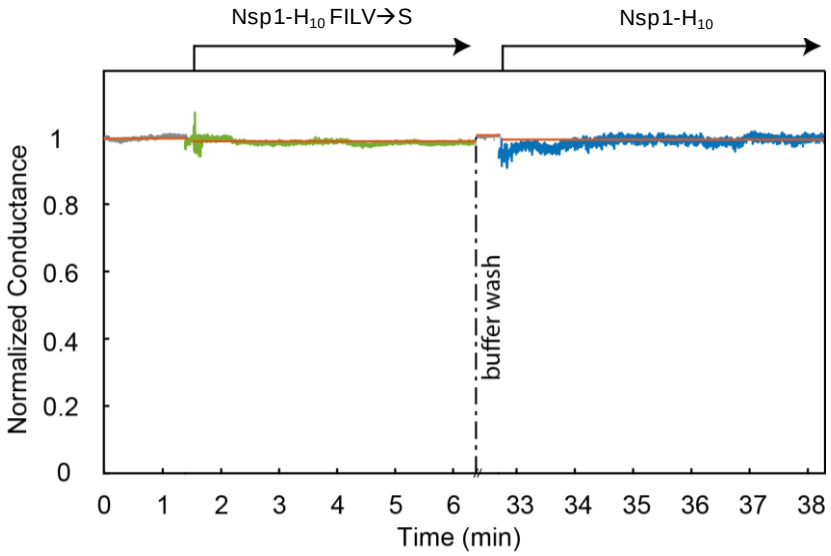

Figure S6. Nsp1-H_{10} proteins do not bind to bare SiN nanopores. Representative ion current traces for bare SiN nanopores of 40 nm diameter. Exposure to Nsp1-H_{10} and Nsp1-H_{10} FILV→S (as indicated) does not affect the conductance level significantly compared to the baseline conductance. Data are presented analogous to Figure 6a. Across triplicates of the set of injections shown, currents changed by less than 5% compared to baseline.

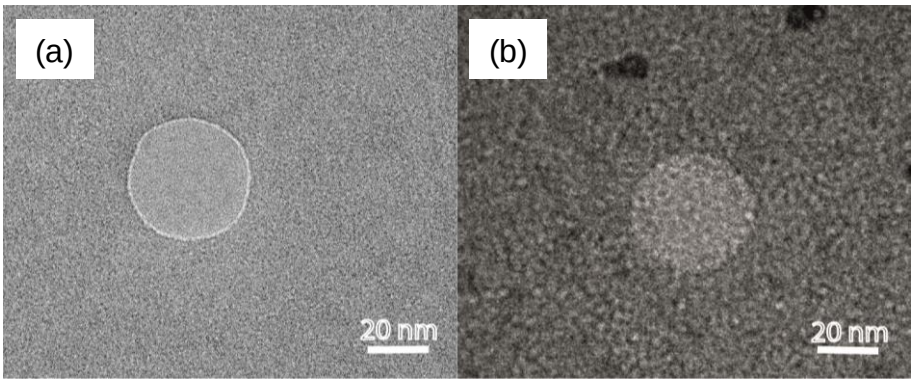

Figure S7. Transmission electron micrographs of nanopores. (a) Bare nanopore of 40 nm diameter. (b) The same nanopore after *in situ* Nsp1-H_{10} coating. In (b), the presence of bio-organic material in the pore and on the SiN membrane surface is evidenced by the grainy appearance which is lacking in (a). Similar images have been reported in a previous study for Nsp1-coated solid-state nanopores.[18c] We emphasize that the exact structural arrangement of the Nsp1 cannot be elucidated from such images because the structure of disordered proteins is generally difficult to resolve, and because the sample has been dried and is imaged in high-vacuum imaging conditions.

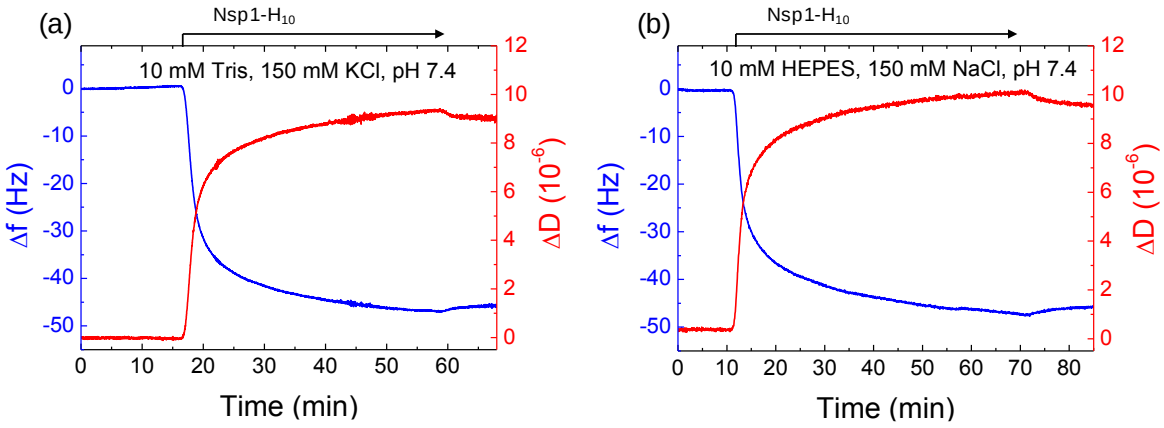

Figure S8. Buffer and cation types do not affect Nsp1 immobilization. Binding of Nsp1-H_{10} FILV→S is shown in (a) 10 mM Tris, 150 mM KCl, and in (b) 10 mM HEPES, 150 mM NaCl, both at pH 7.4. Conditions: Nsp1-H_{10} – 1.5 μM; silica surfaces were functionalized with EDTA and loaded with $NiCl_2$ (2 mM for 15 min) prior to the measurements.